11th International Workshop on Ship and Marine Hydrodynamics
Hamburg, Germany, September 22-25, 2019

The CFD Study of Rudder-Bulb-Fin System in Changing Cambered Foil and AOA Applied to KVLCC2 Tanker

Tho-Quang Truong*, Yasuyuki Toda

Osaka University, Department of Naval Architecture and Ocean Engineering
Suita City, Osaka Prefecture, Japan

*Corresponding author: thoquangtruong@gmail.com

ABSTRACT

The present research is to develop the fin geometry based on an available rudder designed for KVLCC2 tanker in calm water. The improvement of rudder-bulb-fin system is discussed in detail in this paper. The cambered foil that is used in this research is a cambered 4-digit airfoil as a design of the National Advisory Committee for Aeronautics. The mean camber line and thickness have been adjusted and simulated using CFDship-Iowa code to be able to find out the optimal energy-saving devices. The angle of attack is also combined through obtaining its benefit from previous designs. The total resistance by these designs could be reduced a significant percentage amount and improved the propulsive efficiency in comparison with previous designs.

1 INTRODUCTION

The manual goods have been transporting almost by sea transport. Therefore, shipbuilding industry plays an important role in operating the transportation networks. Grasp the reality of the situation; many companies in the world have built series types of cargo ship to meet the needs of the marketplace. However, with the rapid advent of number of new ships, it has led a number of difficulties such as complex systems or environmental pollution. An increasing number of ships in the world has resulted in the degradation of the quality of air and seawater. This is due to the face that the amount of carbon dioxide emission released from ships and industries has increased significantly. Furthermore, since the rapid exhaustion of the earth's natural resources and the increase of fuel oil price, the world is looking at greener ships with lower carbon emission and better fuel efficiency. It became the springboard and the true inspiration for researchers and developers in shipbuilding industry field. Thus, there are many kinds of energy-saving devices (ESDs) around ship stern place are developed and introduced by companies as well as researchers at universities for a few recent decades.

Nguyen et al. (2016) presented several types of rudder with small changing at trailing edge; four rudder models with different wedge shapes; wedge10-beta30, wedge10-beta45, wedge10-beta60 and wedge10-beta30a (in which the first number represents wedge width and the other is angle of wedge) were designed and simulated using a commercial code, Ansys Fluent. The remark was added that when increasing the wedge angle, the drag could be reduced meanwhile the value of lift/drag ratio increased. The wedge10-beta60 rudder gives smaller drag and higher lift/drag ratio compared to the other cases. Kim et al. (2014) developed a ZB-F twisted rudder for a 320m long container ship at 20knots by viscous simulation. They pointed out that the rudder-bulb should not be installed together with contra-rotating propellers as well as propeller boss cap tip. The bulb-fin not only improved the effective wake but gained extra thrust and raised the propulsive efficiency 2.95% as well.

JMU (Japan United Corporation) and MHI (Mitsubishi Heavy Industries, Ltd) designed a counter-rotating propeller that consists of two propellers (rotation about the same axis in opposite directions). A grim wheel was proposed using the central part (turbine shaped) to drive the outer propeller portion. The propulsive efficiency was improved by recovering the energy loss due to rotational flow behind propeller.

The “ultimate rudder” was developed by Nakashima propeller Co., Ltd. The RANS simulation was performed using a commercial CFD code (CRADLE SCRYU/Tetra) with unstructured grids. The rudder-bulb extends upstream and close to propeller boss, using a system that is designed in order that the rudder can be easily rotated. The results of this research show that the hub vortex can be eliminated mostly and the improvement of hull efficiency was 4.1% compared with the normal rudder.

Obtaining the best combination of low resistance and high propulsive efficiency is also one of the goals that we are heading. Generally, this can be attained by proper matching of the ship hull, engine, and propeller or by combination of several ESDs. The authors focused on ESDs for reducing the energy loss as well as gaining extra thrust from propeller rotational flow. The rudder-bulb is known as a popular ESD device for a long time ago in every corner of the world whereas Rudder-Bulb-Fin system (RBFS) is still a relatively new concept. A few kinds of research about RBFS had been reported recently. Kawasaki heavy industries, Ltd. has offered a Rudder-Bulb system with fins, the energy-saving effect of which achieves approximately 2%-7% and had been already applied on many real ships including LNG (liquefied natural gas), LPG (liquefied petroleum gas) and bulk carriers. Matsumoto and Sakamoto (2009) also succeeded in about 2% fuel consumption reduction with a patent dressing a finned rudder. The location of port fin is higher than starboard’s one and the fin length for both sides is not as long as the propeller radius. Among their designs, one type of port side fin was designed with an upward inclination. Compared with the conventional rudder; the experiment showed that the ship required less horsepower in maintaining the same speed. The research (Truong, et al. 2017) was concentrated on the benefit among small changing angles of attack (AOA) which were adjusted from -2 to 1 degree with 1-degree increment for both sides of rudder-fin. Also, several cases such as twisted fin, large changing AOA, cutting starboard side with- and without a dummy propeller mode were simulated by CFDship-Iowa code (Truong, et al. 2018). The research aims to achieve a RBFS that operates with lowest possible drag and highest possible propeller efficiency under different conditions.

2 NUMERICAL METHODS

2.1 Ship Model

The objective ship is KRISO Very Large Crude Carrier 2 which is called KVLCC2 with a model scale of 1:100. The ship model was tested at a design speed of 0.795 m/sec which having the Froude number of 0.142. The geometry of KVLCC2 model can be seen in Figure 1 and important dimensions of ship and propeller are listed in Table 1 below (SIMMAN 2008).

Table 1. Principal particulars of KVLCC2 vessel

Main particulars	Symbol	Full scale	Ship model	Unit
Length between perpendiculars	L_{PP}	320	3.2	m
Breadth at water line	B_{WL}	58	0.58	m
Depth	D	30	0.3	m
Draft (fully loaded condition)	T	20.8	0.208	m
Displacement	∇	312622	0.313	m^3
Block coefficient	C_B	0.8098	0.8098	…
Mid-ship section coefficient	C_M	0.9980	0.9980	…
Propeller				
Diameter	D	9.86	0.0986	m
Expanded blade area ratio	Ae/A0	0.431	0.431	…
No. of blades		4	4	No.
Pitch ratio (0.7R)	p/D	0.721	0.721	
Hub ratio		0.155	0.155	…
Rotation direction		Right hand	Right hand	…

For rudder-fin, the fin is attached on the rudder-bulb for both sides. The suction surface is facing up for port fin and down for starboard fin which is clearly observed in the red area of Fig. 1. When investigating the drag effect on the shape of the rudder-fin and the flow behind the propeller, a number of modifications to the rudder-fin geometry were tested. As it well known, the angle between the flow direction and the chord line is called the AOA and it has a large effect on lift generated by horizontal fins. By considering a decrease of lift, a decision with changing 6-degree attack angle was taken for that purpose.

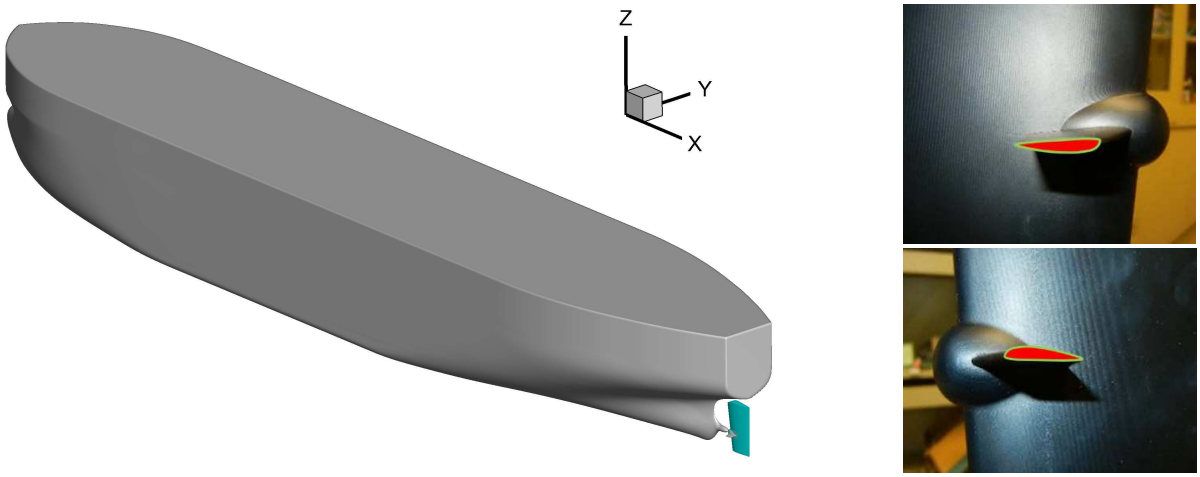

Figure 1. View of KVLCC2 ship model and rudder-bulb-fin (starboard fin [up] and port side fin [down])

2.2 Computational domain, boundary conditions, and grid generation

The non-dimensional computational domain showed in figure 2 with boundary conditions is a rectangular prism and extends range in 3-direction; $-0.5<x/L_{PP}<2.35$, $-1<y/L_{PP}<1$ and $-1<z/L_{PP}<0.22$, where x, y, z are the components of the Cartesian coordinate. The ship bow (FP) is located at $x/L_{PP}=0$ and the stern (AP) is located at $x/L_{PP}=1$. X-coordinate is taken as positive towards the aft of the ship. Y-coordinate is taken positive towards starboard direction and Z is positive in upward direction which can be seen clearly either in Fig. 2 or Fig. 3. The undisturbed free surface is located at $z/L=0$.

For inlet boundary condition, the free inflow velocity is set as non-dimensional ship speed ($u/U_0=1$). The exit boundary condition is used for the outlet. The far-field boundary conditions are implemented on the domain of top and bottom. Zero gradient boundary condition is applied for all the solid surfaces. The detail is described in Table 2 and noted that the rotating hub is considered. With $u/U_0=0$ imposed on the hub surface, the tangential velocity components (v/U_0 and w/U_0) are specified according to the propeller angular velocity: $2\pi r_{hub}n$ where r_{hub} is hub radius and n represents the propeller revolution rate.

Table 2. Boundary conditions

	u	**v**	**w**	**p**	**k**	**ω**
Inlet	U_0	0	0	$\nabla p=0$	10^{-7}	9.0
Outlet	$\nabla^2 u=0$	$\nabla^2 v=0$	$\nabla^2 w=0$	$\nabla p=0$	$\nabla k=0$	$\nabla \omega=0$
Bottom	U_0	$\nabla v=0$	$\nabla w=0$	0	$\nabla k=0$	$\nabla \omega=0$
Top	U_0	0	0	$\nabla p=0$	$\nabla k=0$	$\nabla \omega=0$
Sides	$\nabla u=0$	$\nabla v=0$	$\nabla w=0$	$\nabla p=0$	$\nabla k=0$	$\nabla \omega=0$
No-slip	0	0	0	$\nabla p=0$	0	$\frac{60}{\mathrm{Re}\,\beta\Delta y^2}$

The structured grid was generated using Pointwise software (Pointwise, 2010) and used along with multi-block overset techniques to simplify the grid generation complexity. The whole computational domain consists of 15 overset grid blocks, all the blocks related to the ship body are generated by a hyperbolic grid generator. A propeller disk is needed for propeller modelling. The fins have two overset parts; that is, one side of fin is connected to the rudder-bulb surface and the other side linked to tip. The wake refinement was built surrounding the ship stern to increase grid resolution and background grid that defines the overall domain of the computation and far-field boundary conditions. Since the wall function is not used in this research, the non-dimensional grid size normal to the solid surface is taken as 10^{-6} ($y^+<1$) to capture the boundary layer and turbulence. The grid is finer near water surface and the ship body to get smoother surface deformation. Among the blocks, the numerical connectivity is generated by SUGGAR. To integrate the area, forces and moments properly, USURP (Unique Surfaces Using Ranked Polygons) code is performed to give weights on the cells overlapping on the solid surface. The total grid points are around 9 million and the detail of grids for each block is shown in the following table.

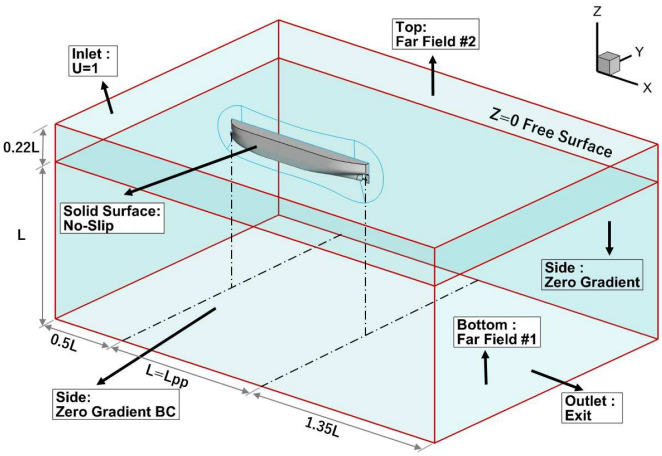

Figure 2. Computational domain and boundary conditions

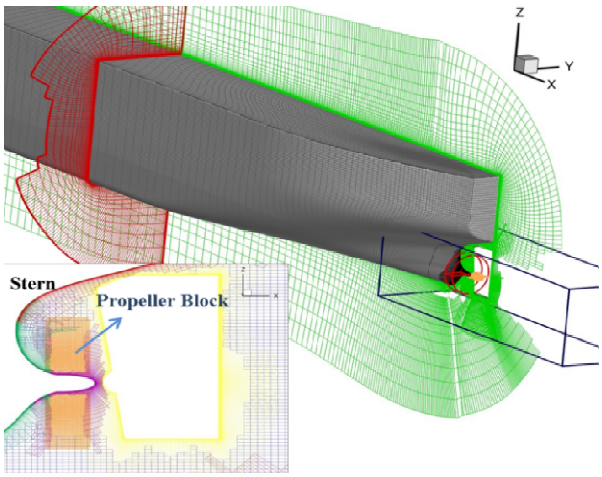

Figure 3. Overset grid system

Table 3. Details of grids

Block name	Type	I_{max}	J_{max}	K_{max}	Total
Hull (port side)	O-grid	154	50	144	1108800
Hull (starboard)	O-grid	154	50	144	1108800
Stern (port side)	O-grid	55	50	40	110000
Stern (starboard)	O-grid	55	50	40	110000
Hub (port side)	O-grid	55	50	40	110000
Hub (starboard)	O-grid	55	50	40	110000
Propeller	O-grid	35	111	105	407925
Rudder(port side)	O-grid	44	45	97	192060
Rudder(starboard)	O-grid	44	45	97	192060
Fin(port side)	O-grid	101	42	47	199374
Tip(port side)	O-grid	101	37	21	78477
Fin(starboard)	O-grid	101	42	47	199374
Tip(starboard)	O-grid	101	37	21	78477
Wake refinement	H-grid	151	81	81	990711
Background	H-grid	216	121	151	3946536
Total					8 942 594

CFDship-Iowa version 4.5 is a dynamic overset URANS (Unsteady Reynolds-Averaged Navier-Stokes) solver coupling with 6 degrees of freedom (DOF) motion solver specifically designed for ship application. The URANS solver is based on finite difference method and using the structured grid in this research. A two-equation k-ω shear stress transport (SST) turbulence model with no wall function was used to describe the turbulence and projection method is used for pressure-velocity coupling. The free surface is given by a single-phase lever-set method and its location is given by 'zero' value of the level-set function φ, positive in water and negative in air. In the CFDship-Iowa code, the ship motions (heave and pitch) were solved in non-inertial ship coordinates and the flow field was solved in absolute inertial earth coordinates (Wilson et al., 2006). Because refining the mesh involved longer time for converging, these motions were fixed in order to get faster convergence in these simulations.

2.3 Propeller model

The simulations were performed with and without propeller effect to obtain total resistance and self-propulsion factors. For with-propeller cases, the body force propeller model based on the quasi-steady assumption and blade element theory (BET) using the total velocities (u/U_0, v/U_0, w/U_0). The velocities are provided by URANS solver were used as the inflow to calculate the lift and drag on each blade element (as shown in Fig.4). Propeller's parameters such as pitch angle and chord length distribution are applied when running the simulations. The lift coefficient is obtained by $C_L=2\pi k_1 \sin\alpha$, where k_1 is an empirical correction for finite blade width and α is the AOA against the zero-lift line. Drag coefficient is constant value as

C_D=0.02. The local thrust (dT) and torque (dQ) on each blade element inside the propeller disk (cylindrical block) can be calculated from C_L and C_D. The longitudinal and tangential body forces (fb_x, fb_θ) would be based on the average effect of dT and dQ among N blades, propeller rotation perimeter ($2\pi r$) at certain radius (r) and propeller thickness (Δx).

$$fbx = \frac{dT.N}{\Delta x.2\pi r} \tag{1}$$

$$fb_\theta = \frac{dQ.N}{\Delta x.2\pi r^2} \tag{2}$$

The quasi-steady assumption effect is useful in ship applications since propeller rotates at high speed for many cases such as seakeeping and ship maneuvers. The momentum equations in URANS solver would be solved along with those body forces as the source terms. The components of total propeller forces and moments would be considered in the equations of motions in the 6DOF solver. Several coordinate transformations are required in the code since the flow field, 6DOF motion and the propeller are solved in earth coordinate, ship coordinate and shaft of propeller coordinate, respectively.

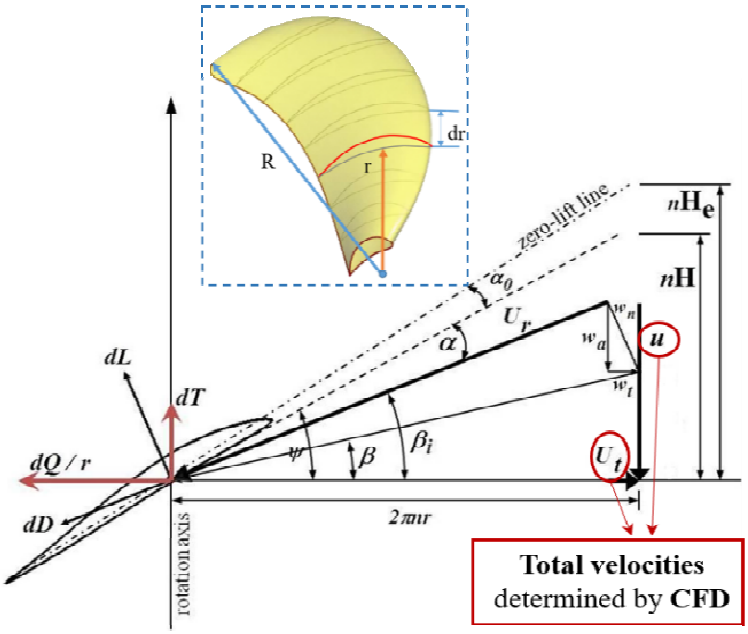

Figure 4. Blade element theory

The concept of using total velocities is useful in many kinds of ship applications as well. The main advantages are: (1) induced velocity subtraction is not required, (2) free vortex is not assumed and fixed. In traditional propeller code, the governing equation is Laplace's equation: $\nabla^2\phi = \nabla\vec{u} = 0$ with boundary condition $\hat{n}.\vec{u}$=0 based on potential flow theory. Since when coupling the propeller code and URANS, a procedure or technique of induced velocity subtracting is required as mentioned by Simonsen and Stern (2005). The inflow velocity becomes known after subtracting induced. The unknown induced velocity $\vec{u}_{induced}$ can be solved by known normal vector $\hat{n}$ on body geometry and inflow velocity $\vec{u}_{inflow}$ via a linear system $[\hat{n}][\vec{u}_{induced}]=[-\hat{n}.\vec{u}_{inflow}]$. In the next step, there are many methods to solve induced velocity; for instance, small perturbation method like lifting line and lifting surface/vortex lattice method, or panel method/boundary element method based on Green's third identity. In most of those methods, the induced velocity on body geometry is induced by bound vortex and free vortex which is a linear superposition, i.e. $\vec{u}_{induced}= \vec{u}_{bound\text{-}vortex} + \vec{u}_{free\text{-}vortex}$. The strength of bound vortex is unknown on body geometry. It means that the helical pitch and shedding direction of free vortex have to be assumed and fixed in a certain shape. The induced velocity subtraction is not needed anymore since the total velocity is used. The free vortex is included in the total velocity solved by RANS and the bound vortex strength would be solved in the propeller code. It is possible to implement this concept in any inviscid propeller code such as: $[\hat{n}][\vec{u}_{bound\text{-}vortex}] = [-\hat{n}.\vec{u}_{RANS}]$, i.e. $\vec{u}_{RANS}= \vec{u}_{free\text{-}vortex} + \vec{u}_{inflow}$. It is beneficial for applying the propeller model to the present work because the free vortex would be disturbed by the rudder and energy-saving devices.

2.4 Fin-foil

There are many kinds of fin-foil developed and introduced by the National Advisory Committee for Aeronautics (NACA) and its benefits are different. The cambered 4-digit NACA foil had been chosen in the research of this time. The mean camber line is calculated by the formula as follows:

$$y_c = m\frac{x_c}{p^2}(2p - \frac{x_c}{c}) \qquad \text{for } 0 \le x < p \tag{3}$$

$$y_c = \frac{m}{(1-p)^2}(1 - 2p + 2px - x^2) \qquad \text{for } p \le x \le 1 \tag{4}$$

Where: m is maximum ordinate of the mean line in fraction of the chord (first digit)
p represents the location of maximum camber divided by 10 (second digit)

The fin-foil has a maximum camber of 5 percent located at the position of 40 percent of chord from the leading edge with a maximum thickness of 12 percent as a fraction of the chord (hereinafter, NACA 5412). The position of upper points (x_u, y_u) and lower points (x_l, y_l) are defined by the following relationship and plotted in 2D Cartesian coordinate as shown in Figure 5.

$$x_u = x_c - y_t \sin\theta \qquad x_l = x_c + y_t \sin\theta$$
$$y_u = y_c + y_t \cos\theta \qquad y_l = y_c - y_t \cos\theta$$

Where y_t is thickness distribution and $\theta = \tan^{-1}(\frac{dy_c}{dx_c})$

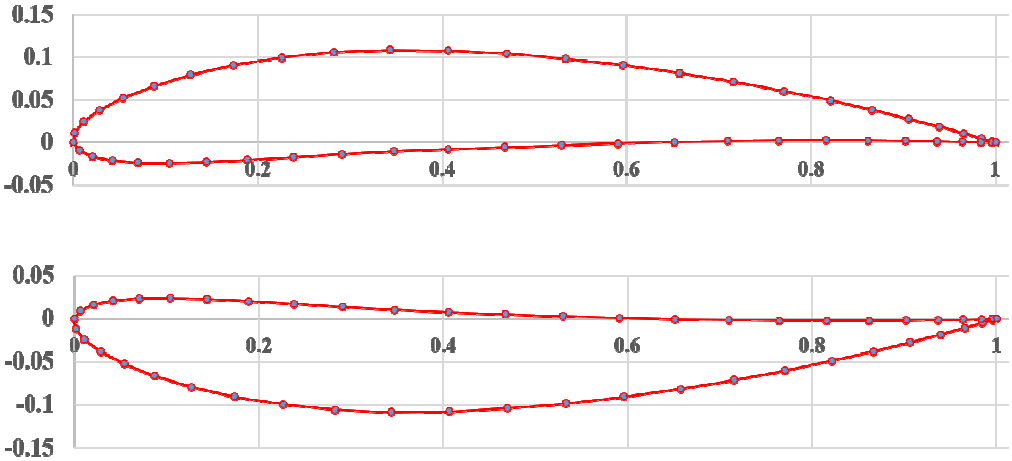

Figure 5. Fin-foil section of NACA5412
[upper curve for portside and lower curve for starboard]

Note that the fin-foil at the end of tip still maintains as the shape of the original one. The fin-lets might reduce the fin-tip vortices and increase the efficiency of fin. In this research, the cap of tip was rounded end in order to slightly improve the efficiency of the end of the fin. The result of five kinds of RBFS in changing cambered foil and adjusting AOA will be shown:

- The NACA5412 (1) which has only a new camber line (hereinafter NACAps0_sb0)
- The NACA5412 (2) which has a new camber line and starboard fin is rotated 1-degree up (hereinafter NACAps0_sb1)
- The NACA5412 (3) which has a new camber line and starboard fin is rotated 6-degree up (hereinafter NACAps0_sb6)
- The NACA5412 (4) which has a new camber line and starboard fin is rotated 1-degree up and port side fin is rotated 1-degree down (hereinafter NACAps1_sb1)
- The NACA5412 (5) which has a new camber line and starboard fin is rotated 6-degree up and port side fin rotated 6-degree down (hereinafter NACAps6_sb6)

3 NUMERICAL RESULTS

3.1 Self-propulsion factors

The total resistance has many components in rough sea conditions but the main resistance (in this research) acting on the hull is frictional and viscous pressure. The existence of fin and changing AOA are the cause of raising in the viscous pressure resistance but drop in frictional resistance value or vice versa. The thickness and size of fin are considered since the appearance of fin accompanied in increasing wetted area. The total resistance R with and without propeller for model scale is calculated from the predicted total resistance coefficient (C_t) and the relationship is as follows:

$$R = 0.5C_t.\rho.U_0^2.A \tag{5}$$

In which density ρ =998kg/m^3, A is the total surface wetted area for whole ship.

The propeller revolution rate equals 16.3 rps which is obtained by the self-propulsion test in the experiment with the fully loaded condition. The total resistance with propeller and the final converged thrust and torque coefficients are listed in Table 4 to five-digit accuracy which are averaged from the simulate output.

Table 4. Total resistance and thrust, torque coefficients comparison

Resistance and coefficients	R [N]	K_T	$10K_Q$
NACAps0_sb0	5.4736	0.1977	0.2163
NACAps0_sb1	5.4379	0.1977	0.2163
NACAps0_sb6	5.4956	0.1976	0.2162
NACAps1_sb1	5.4367	0.1977	0.2163
NACAps6_sb6	5.4329	0.1977	0.2163

Based on the value of total resistance and EFD open water characteristics curve, the self-propulsion factors were determined by Eqs 6~7 and the value illustrated in Figure 6.

$$t = \frac{R_T - R_0}{T} \tag{6}$$

$$1 - w = \frac{Ja}{Js} \tag{7}$$

Where R_T is total resistance with propeller, R_0 is total resistance in the case of absence propeller, J_a and J_s are the advanced coefficients; J_a is obtained from the open water characteristics curve while J_s equals 0.495.

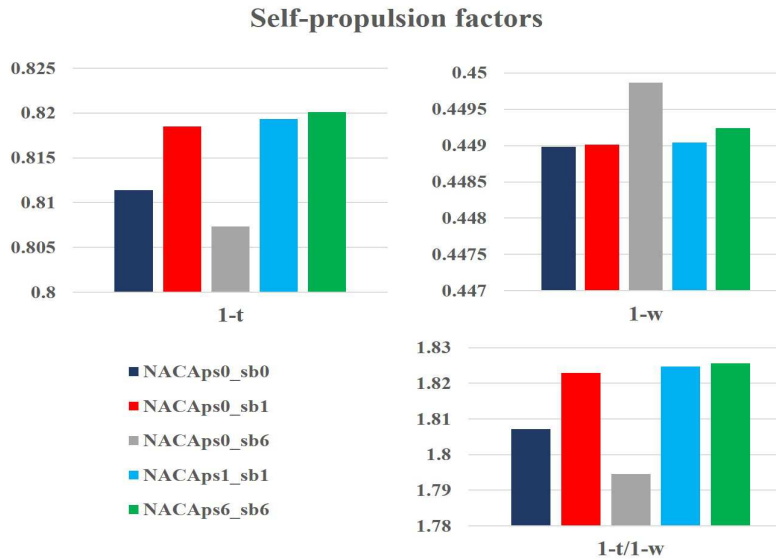

Figure 6. Computational self-propulsion factors

The ratio η_H=1-*t*/1-w is often called the hull efficiency, and we know that a large thrust deduction (1-*t*) and a small wake fraction (1-w) are beneficial effect. The total resistance of NACAps6_sb6 case with propeller could be reduced with changes in increasing of (1-*t*) factor, 5.25% and decreasing of (1-w) factor by 0.78%. Thus, the hull efficiency value of NACAps6_sb6 is highest so far, in comparison with normal fin. Compared with *R*=5.784N (with propeller) for normal rudder, the total resistance could gradually reduce by these designs, especially around 6 % by NACAps6_sb6 case.

3.2 CFD flow field

In fact, there are many options to choose stations in order to analysis the wake field behind the rotating propeller; in this research, the main interest to show flow field is the downstream area at x/L_{PP}=1 (AP) and x/L_{PP}=1.025 (behind the trailing edge of rudder) whereas the propeller center is located at the station of x/L_{PP}=0.9875. The Figs 7~11 show the axial velocity contours (u/U_0) and cross flow vector (v/U_0, w/U_0) for normal rudder and NACA5412 with different changing AOA. The flow fields are extracted on the section at x/L_{PP}=1 (AP position) across the rudder-fin surface (looking from stern to bow). The axial velocities are accelerated by the propeller to 1.6 times ship speed. The basic flow features were similar for almost cases since the geometries are slightly changed only. The hub vortex would trend to move to the left side and its location is lower due to the rotating hub and bulb. Also, the propeller rotational flow vortex attaches on the port side surface of the rudder and a downward flow is caused on the starboard side surface. The vortices are truncated by fins, especially the starboard side one. Two eddies appear on the lower and upper starboard fin, a bit away from the rudder, e.g. y/L_{PP}~0.01, is induced by the downward flow. The result for those cases has not been validated by Experimental Fluid Dynamics (EFD) but the accuracy of the numerical method for the similar object had already been proved by comparing with the experimental data which were shown in previous papers (Truong et al., 2017, 2018).

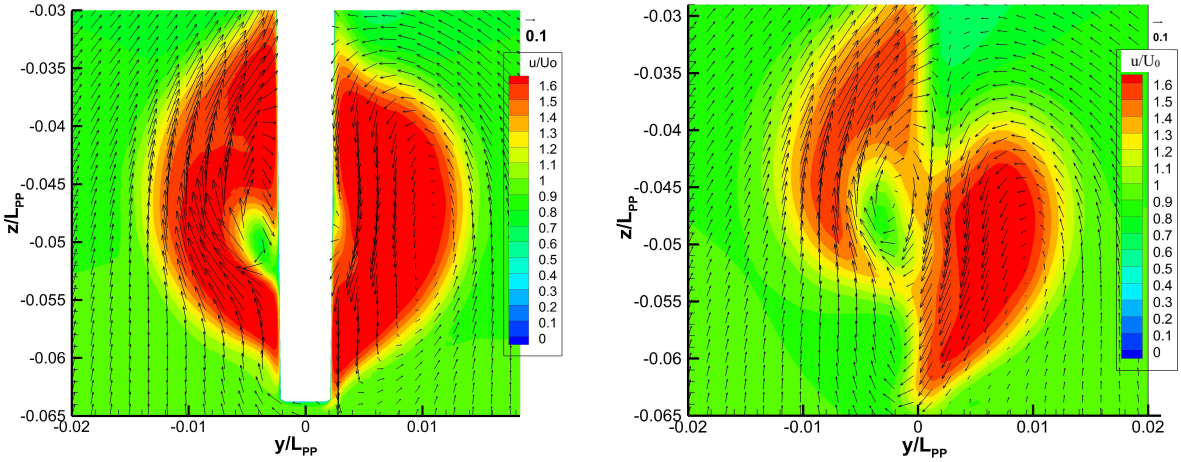

Figure 7. Axial velocity profiles and cross flow vector at x/L_{PP}=1 and x/L_{PP}=1.025 for normal rudder [looking from stern to bow]

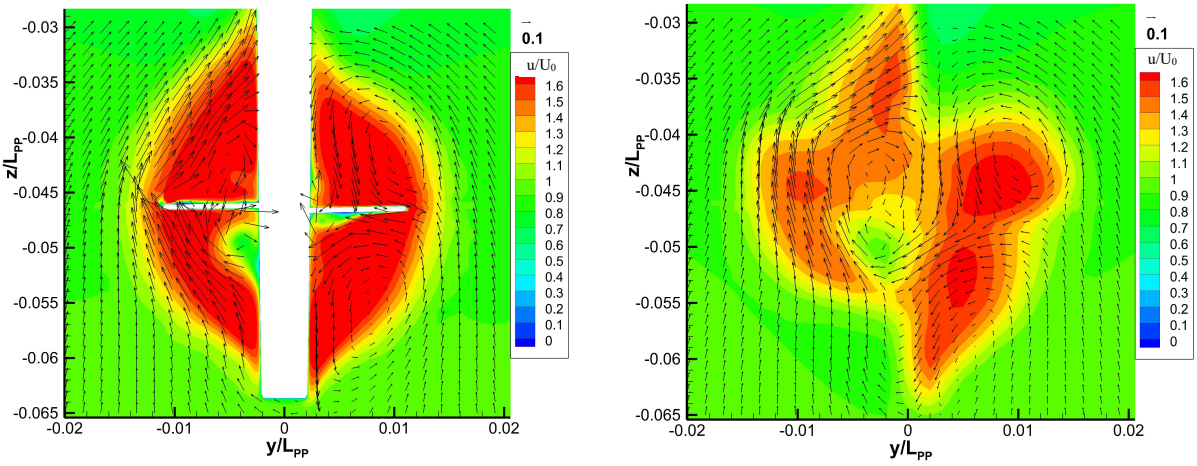

Figure 8. Axial velocity profiles and cross flow vector at x/L_{PP}=1 and x/L_{PP}=1.025 for NACAps0_sb0 [looking from stern to bow]

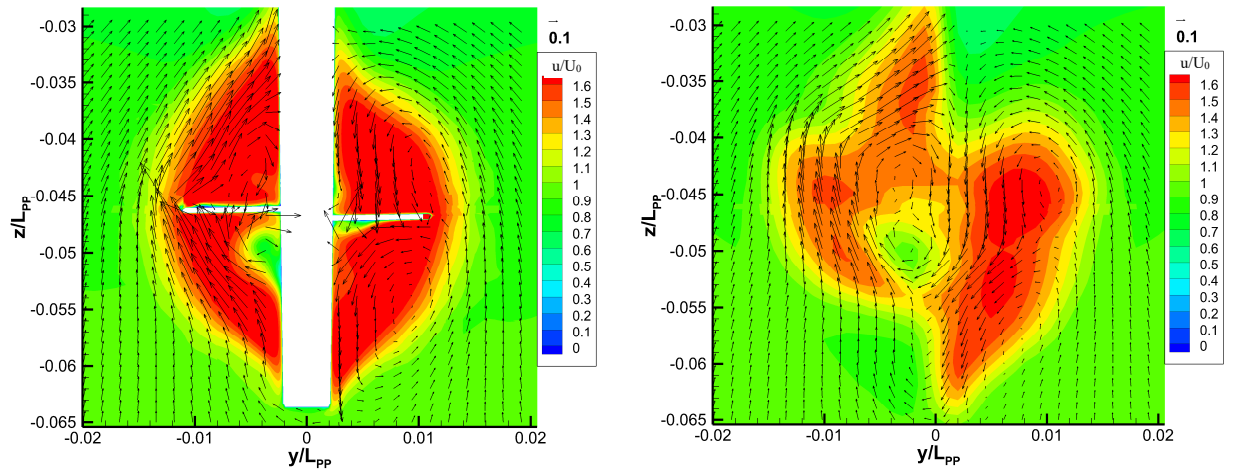

Figure 9. Axial velocity profiles and cross flow vector at $x/L_{PP}=1$ and $x/L_{PP}=1.025$ for NACAps0_sb6 [looking from stern to bow]

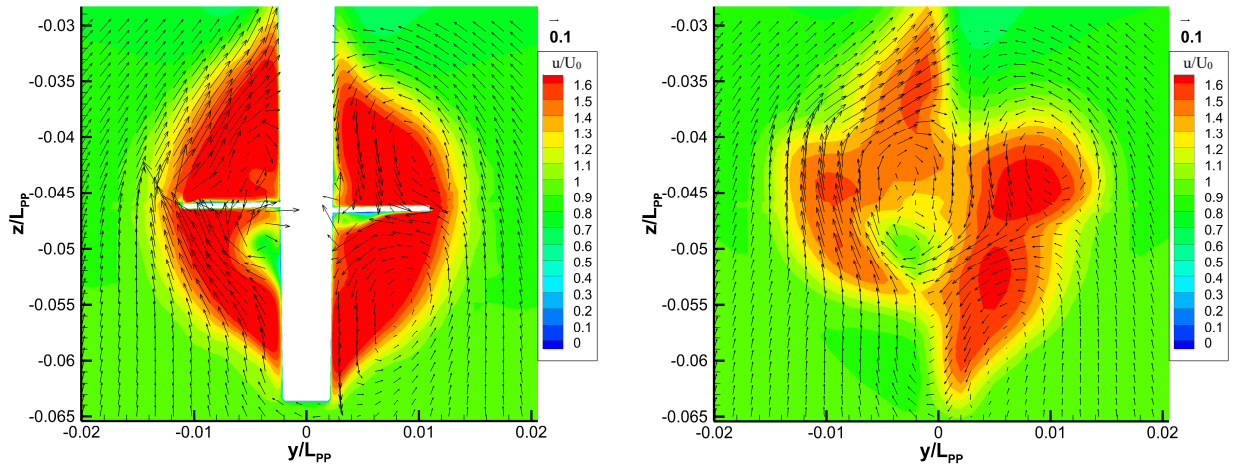

Figure 10. Axial velocity profiles and cross flow vector at $x/L_{PP}=1$ and $x/L_{PP}=1.025$ for NACAps1_sb1 [looking from stern to bow]

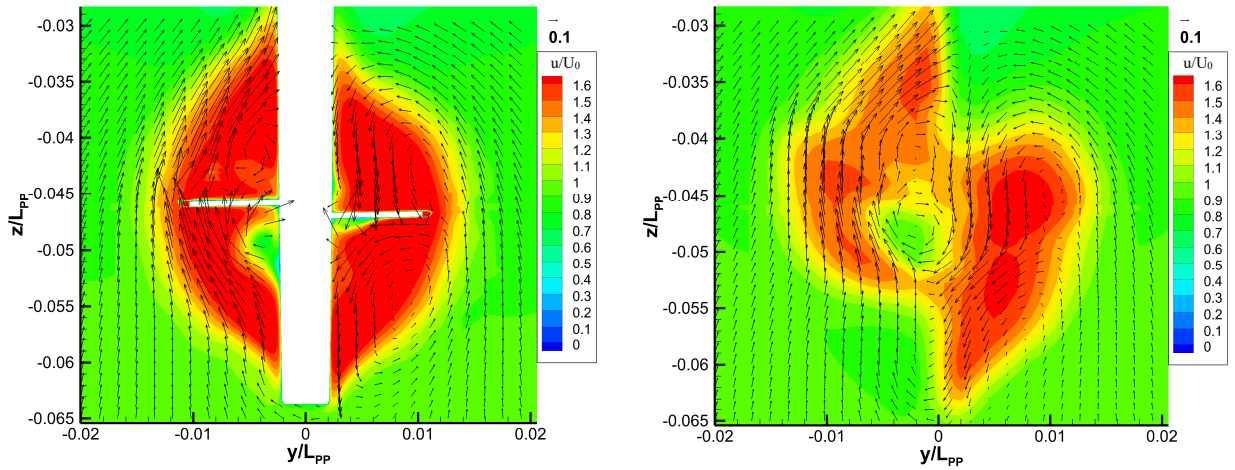

Figure 11. Axial velocity profiles and cross flow vector at $x/L_{PP}=1$ and $x/L_{PP}=1.025$ for NACAps6_sb6 [looking from stern to bow]

In the following, flow separation and streamline had been added as more evidence in order that further strengthen persuasiveness of this study. Fig. 12 draws the axial velocity contours limited to $u/U_0=1.1$ and streamlines at $y/L_{PP}=0.005$ (at the red line near the bulb) section on the starboard side fin. Flow separation results in changing drag; in other words, the smaller flow separation means smaller drag and flow field is improved. The dark blue area (red rectangular) indicates large flow separation and reverse flow. When comparing the size of the dark blue region, it is obvious that the flow separation and reversed flow are completely disappeared in the case of NACAps6_sb6 on section of $y/L_{PP}=0.005$

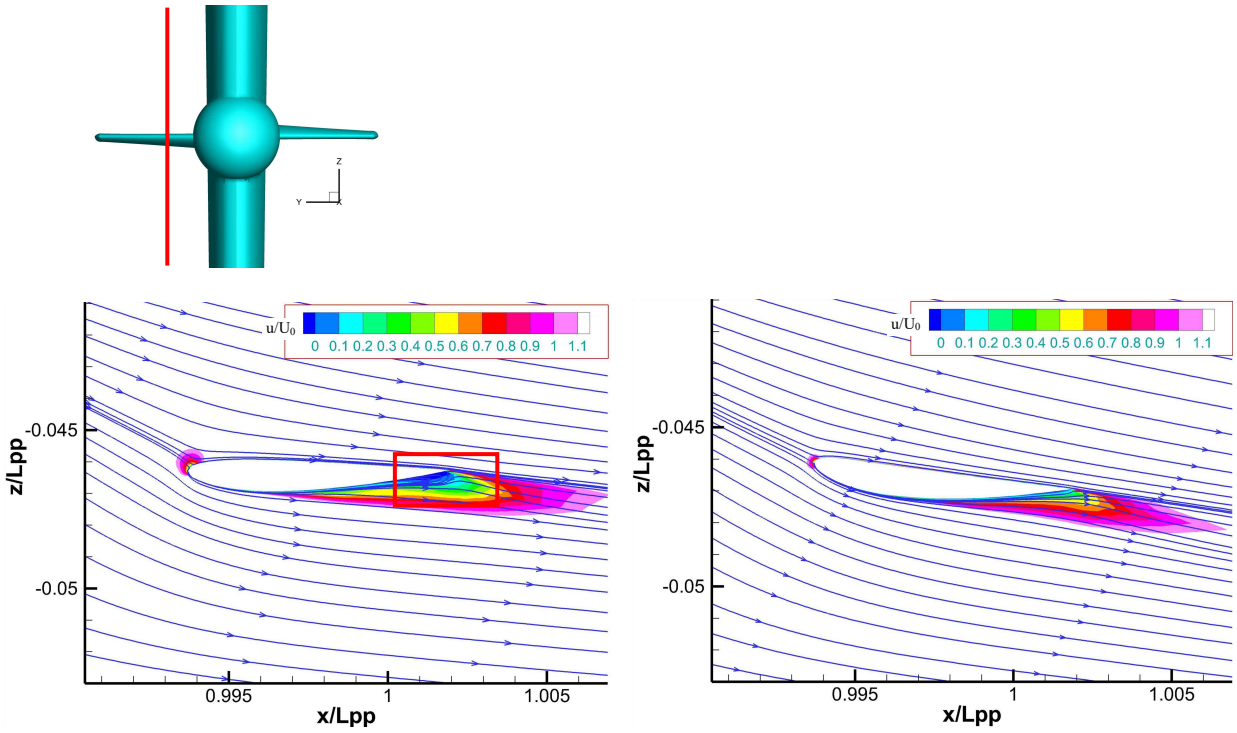

Figure 12. Velocity contours and streamlines for starboard side of original fin [left] and NACAps6_sb6 [right]

3.3 Vortex shedding

S_{ij} is known as the rate-of-strain tensor and Ω_{ij} is the vorticity tensor. The Q-Criterion is one of the three invariants of the velocity gradient tensor and obtained by equation 10, written below. The Q-criterion represents the local balance between shear strain rate and vorticity magnitude, defining vortices as areas of which the strain-rate magnitude is smaller than the magnitude of vorticity.

$$S_{ij} = \frac{1}{2}\left(\frac{\partial u_i}{\partial x_j} + \frac{\partial u_j}{\partial x_i}\right) \tag{8}$$

$$\Omega_{ij} = \frac{1}{2}\left(\frac{\partial u_i}{\partial x_j} - \frac{\partial u_j}{\partial x_i}\right) \tag{9}$$

$$Q = \frac{1}{2}\left(\left|\overline{\Omega_{ij}}\right|^2 - \left|\overline{S_{ij}}\right|^2\right) \tag{10}$$

In order to understand the turbulence structure, the flow structures are illustrated using the Q-Criterion with Q=5000 colored by the axial velocity contours for normal rudder and NACAps0_sb0. The Q-Criterion iso-surface is visualized only for NACAps0_sb0 because the Q-Criterions are not big difference among cases. Also, the Q-Criterion of normal rudder is added so that easily compared to new designs. The main turbulence structure to be captured well in the simulation. Due to the use of average effect in body-force model of the propeller, only the ring-shape can be seen in the following figures. It is clearly seen that the hub vortex was split by the fins. However, it looks the portside fin does not affect to the main port hub vortex (the arrow in red). The bigger hub means the propulsion energy of the propeller decreases. From that point of view, changing the position of portside fin is necessary in order to make the flow smooth.

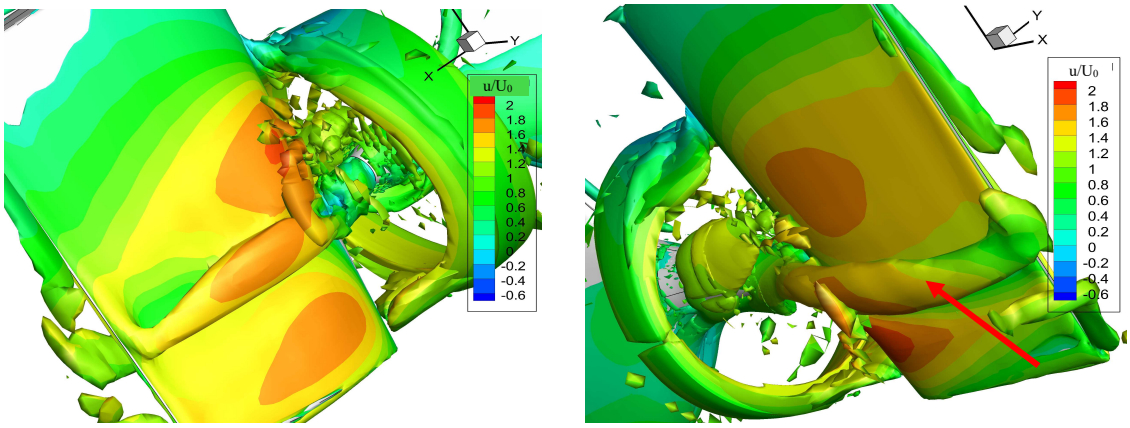

Figure 13. Turbulence structures of flow around stern for normal rudder (starboard side [left] and portside [right])

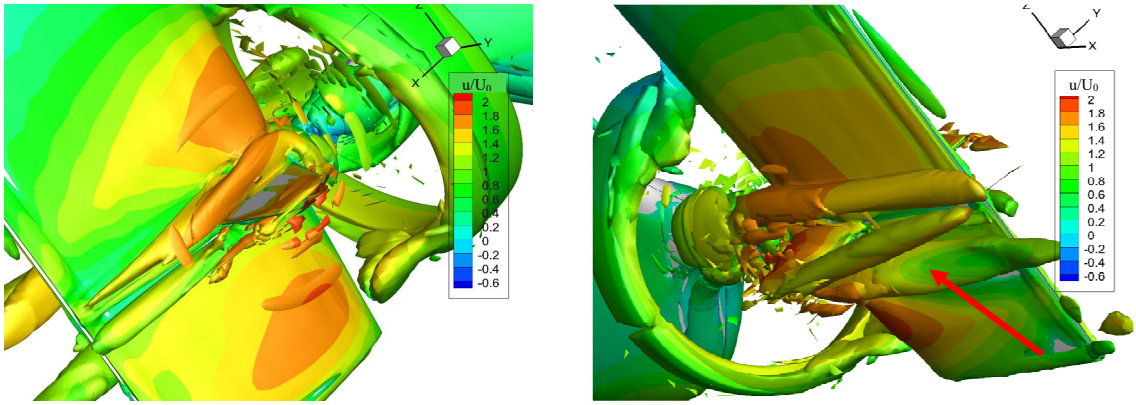

Figure 14. Turbulence structures of flow around stern for NACAps0_sb0 (starboard side [left] and portside [right])

3.4 Pressure distribution

Wide understanding related to pressure problem is one of the keys for designers to develop new projects. The pressure is the most dynamic variable in fluid mechanics; of course following the velocity. Pressure drag is caused by the pressure different along fin upper and lower surfaces as it travels through the fluid. Figure 15 shows the pressure distribution on the rudder-fin surface of those NACA5412 cases and it can be observed that those pictures display two high-pressure regions near the leading edge of the rudder as well as two high-pressure areas on the upper starboard surface and the lower port side fin surface which correspond to the axial inlet velocities. The NACAps0_sb0 case has the strong negative-pressure (blue region) on the upper portside and lower starboard side; on the other hand, the negative pressure on those surfaces dissipated in the case of NACAps0-sb6 and especially NACAps6-sb6 on both sides. The low-pressure region is very small and therefore considerable changes in drag; in other words, the dissipation of negative pressure is the cause of improvement of propeller efficiency.

4 CONCLUSION

The effect of RBFS to wake flow field was investigated by numerical method, CFDship-Iowa version 4.5. The research results proved that the foil fin and attack angle have a large effect on lift generated by horizontal fins, namely NACA5412ps6_sb6, hence a result of increasing the propulsion performance. The total resistance of NACAps6_sb6 case with propeller could be reduced by 4.36 percent with changes in increasing of thrust deduction (1-t) factor, 5.25% and decreasing of wake (1-w) factor by around 0.78 percent. Thus, the hull efficiency value of NACAps6_sb6 is highest so far, in comparison with normal fin. In the event of new designs, the flow around trailing edge of fin was improved with a disappearance of backflow. One more advanced feature is that the system is not only for new ship but can be also easily applied to existing vessels. Nevertheless, inside the propeller disk area, the hub vortex is generated by the propeller acceleration flow, shifted to the port side and other vortexes appear on the starboard rudder. The optimum position of the fins to reduce the total resistance and eliminate the strength of hub vortex will be investigated in the next stage of research. The experiments will be also considered and carried out to assess the validity of the presented results.

ACKNOWLEDGEMENTS

This research was partially supported by U.S. ONR Global NICOP grant N62909-16-1-2015 and the first author research was supported by the Ministry of Education, Culture, Sports, Science and Technology Japan (MEXT) scholarship.

REFERENCES

[1] Ira H. Abott and Albert E. Von Doenhoff "Theory of wing sections"
[2] Matsumoto, D and Sakamoto, T (2009) "Finned Rudder", Patent EP2110311A3
[3] Nguyen, TV, Ikeda, Y (2016) "Hydrodynamic Characteristics of High Lift Rudders with Wedge Tails," *Asia-Pacific Hydrodynamics conf,* AP-hydro, Hanoi, 238-245.
[4] Simonsen, C and Stern, F (2005) "RANS maneuvering simulation of Esso Osaka with rudder and a body-force propeller," *J of Ship Research*, 49(2), 98-120.
[5] Truong, TQ, Wu, PC, Aoyagi, K, Koike, K, Akiyama, Y and Toda, Y (2017) "The EFD and CFD study of Rudder-Bulb-Fin System in Ship and Propeller Wake Field of KVLCC2 Tanker in Calm Water," *Proc 27th Int Offshore and Polar Eng Conf*, San Francisco, ISOPE, 823-830.
[6] Truong, TQ, Wu, PC, Kishi, J, Toda, Y (2018) "Improvement of Rudder-Bulb-Fin System in Ship and Propeller Wake Field of KVLCC2 Tanker in Calm Water," *Proc 28th Int Offshore and Polar Eng Conf*, Hokkaido, ISOPE, Vol III, 184-190
[7] Wilson, R, Carrica, PM, and Stern, F (2006) "Unsteady RANS method for ship motions with application to roll for a surface combatant," Computers & Fluids, 35, 501-524.
[8] https://global.kawasaki.com/en/mobility/marine/technology/energy_saving.html.
[9] https://www.nakashima.co.jp/eng/product/ultimate_rudder.html.

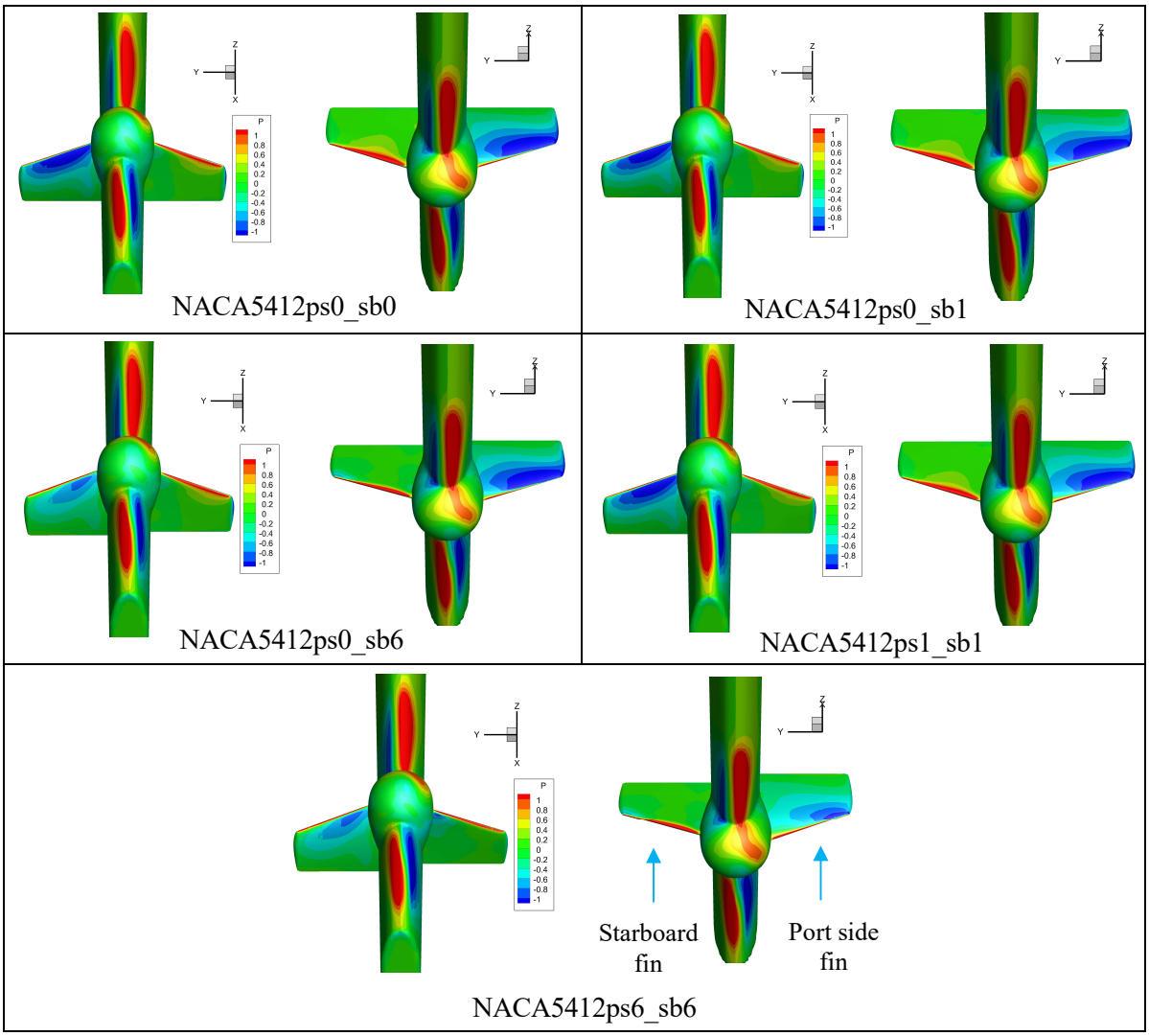

Figure 15. Comparison of pressure distribution on Rudder-Bulb-Fin surfaces